Photodiagnosis and Photodynamic Therapy 23 (2018) 295–305

Contents lists available at ScienceDirect

Photodiagnosis and Photodynamic Therapy

journal homepage: www.elsevier.com/locate/pdpdt

Pegylated hollow gold-mitoxantrone nanoparticles combining photodynamic therapy and chemotherapy of cancer cells

Armin Imanparast[a,b], Maryam Bakhshizadeh[c], Roham Salek[d], Ameneh Sazgarnia[a,b,*]

[a] Medical Physics Research Center, Mashhad University of Medical Sciences, Mashhad, Iran
[b] Department of Medical Physics, Faculty of Medicine, Mashhad University of Medical Sciences, Mashhad, Iran
[c] Torbat Heydariyeh University of Medical Sciences, Torbat Heydariyeh, Iran
[d] Department of Radiotherapy and Oncology, Cancer Research Center, Mashhad University of Medical Sciences, Mashhad, Iran

ARTICLE INFO

Keywords:
Hollow gold nanoshell
Mitoxantrone
Photodynamic therapy

ABSTRACT

Background: In recent years, Mitoxantrone (MTX) has been introduced as a chemotherapy drug which also serves as a photosensitizer and radiosensitizer. Due to its serious side effects, there are limitations to the application of MTX so scientists are looking for solutions to overcome this problem. Hollow gold nanoparticles (HAuNP) have attracted growing attention due to their unique physical-chemical properties, such as biocompatibility, tunable plasmonic absorption peak ranging from visible to near infrared, high stability and various medical applications in imaging, drug delivery and combinational cancer treatments. In this paper, the combinational effect of photodynamic therapy (PDT) and chemotherapy of MTX conjugated to HAuNP is studied.

Method: After optimizing the synthesis of PEGylated HAuNP and preparing nanostructures conjugated with MTX, the characteristics of pharmacological agents including MTX, HAuNP, mPEG-HAuNP,and MTX-mPEG-HAuNP and their toxicity were determined at different concentrations on two cell lines of DFW and MCF7 derived from human melanoma and breast cancer, respectively. To select the optimal concentration for PDT, the cytotoxicity of agents was investigated at concentrations of 3, 6, 9 and 12 μM. Moreover, a LEDs system at 630 nm and power output of 3 W was used to apply PDT process. MTT test was used to determine cell survival 24 h after treatment. Several indexes were utilized for data comparison, such as therapeutic efficacy (TE), necessary concentration to kill 50% of cells (IC_{50}), and necessary light exposure to induce 50% cell death (ED_{50}).

Results: LED exposure alone did not cause significant cell death. For MTX-mPEG-HAuNP, at both cell lines, IC_{50} had the least exposure to dark condition with an exposure time of less than 9 min and this nanostructure had the smallest ED_{50} in each cell line at all concentrations. TE of MTX-mPEG-HAuNP at different exposures and concentrations was greater than 1 for the DFW cells. It was also true for concentrations greater than 6 μM with irradiation times longer than 3 min for MCF7 cells.

Conclusion: This is the first paper to use PEGylated hollow gold nanoparticles as the nanocarrier for MTX. The results indicated that MTX-mPEG-HAuNP improved the efficacy of PDT with Light Emission diode.

1. Introduction

Photodynamic therapy (PDT) is a minimally invasive treatment that can remove tumor cells selectively. PDT consists of three essential components: photosensitizer (PS), tumor oxygen level and ratio of optical wavelength to PS. None of these factors is toxic individually, but together they initiate a photochemical reaction that involves reactive oxygen species (ROS) and singlet oxygen ($^1O_2$), which can generate significant cytotoxicity, leading to cell death by apoptosis or necrosis within the target tissue. ROS and singlet oxygen are highly reactive and have a short half-life. Accordingly, PDT can directly affect those biological substrates closest to the region that produce the species. Therefore, PS localization is a major factor in the study of PDT. The choice of an appropriate light source in the process of PDT depends on the photosensitizer absorption band, the type of disease, localization, and width of therapeutic target. Therefore, the optimal combinations of light source, PS and sufficient oxygen are crucial for successful PDT process. Studies have utilized a variety of light sources like lasers, xenon lamps and light emission diodes (LEDs), reporting a relatively similar efficiency for PDT. Light emitting diodes (LEDs) have been

* Corresponding author at: Medical Physics Research Center, Mashhad University of Medical Sciences, Mashhad, Iran.
E-mail address: sazgarniaa@mums.ac.ir (A. Sazgarnia).

https://doi.org/10.1016/j.pdpdt.2018.07.011
Received 5 February 2018; Received in revised form 13 July 2018; Accepted 18 July 2018
Available online 23 July 2018
1572-1000/ © 2018 Elsevier B.V. All rights reserved.

proposed as an alternative source of light for PDT [1–3].

The major advantages of LEDs include high power output, illumination of large areas, low risk, minimum space occupation, thermal non-destructivity, flexibly arrangement according to anatomical geometry, low cost and availability. Compared to other light sources of PDT, LEDs can have various clinical applications due to their high intensity and large coverage area (approximately 20 cm^2) at one time [4,5].

In recent years, considering the toxicity of antineoplastic drugs for normal tissues, the use of chemotherapy for cancer treatment has been restricted [6]. Many anticancer drugs do not demonstrate therapeutic effects due to poor stability, low solubility, non-specificity, and easy removal by metabolism. As a chemotherapeutic agent, MTX has been used for the treatment of various malignancies, including metastatic breast cancer, non-Hodgkin's lymphoma, and acute myeloid leukemia. MTX uses biological mechanisms to prevent cell proliferation including the disruption of DNA repair/synthesis and inhibition of topoisomerase II and mitochondrial pathway, which ultimately result in apoptosis [7]. MTX has fascinating chemical and physical properties. Montazer Abadi et al. reported the optical and radiation properties of MTX for the first time, proving that MTX can also be used as photosensitizer and radiosensitizer [8].

Conjugation of anticancer drugs to the appropriate nanocarrier can extend the half-life of the drug in the body and control the process of drug release. The ideal drug carriers should possess special features such as chemical stability, long half-life, none or low toxicity, biodegradation capabilities and high conjugation capacity [9]. In particular, functionalized nanostructures with the ability to encapsulate or conjugate drugs are more advantageous than free drugs, providing benefits such as lower drug toxicity, higher targeting efficiency and prolonged half-life, creating new paths to overcome challenges associated with chemotherapy and photodynamic therapy [10].

Among many nanoscale materials, hollow gold nanoparticles (HAuNP) represent an excellent candidate for drug delivery due to their cavity structure, high availability of internal and external surface, good biological safety, biocompatibility and functional ability [11]. The surface plasmon absorption band of HAuNP can be tuned by adjusting the inside diameter and thickness of the gold shell in visible to near-infrared range. Due to their unique physical properties and low toxicity of HAuNP, they have multifunctional nanostructures in medical applications. As contrast agents, biological compounds of HAuNP are used to identify and image cancer cells in vitro and solid tumors of the body (Fig1). Designed for photothermal agents to induce thermal necrosis of tumors, HAuNP has been successfully used in animal studies [12].

PEGylation process helps nanomaterials escape from the immune system. The PEG group is responsible for the solubility of nanoparticles in water, reducing absorption by proteins and providing nanostructured surfaces as an amphiphilic environment for insoluble drugs in the water. When neutral hydrophilic polymers bind with foreign proteins, a lower immune response in the body is stimulated. This phenomenon, known as stealth effect, offers a simple and effective way to increase the stability of nanoparticles. Also, PEGyaltion of nanocarriers leads to increased conjugation efficiency and reduce the unnecessary release of the drug [13,14].

In this study, HAuNP was used to encapsulate the mitoxantrone (MTX), and using different radiant exposures of the light emission diode (LED) at different concentrations of therapeutic agents, the combinational effect of photodynamic and chemotherapy was studied. The main innovations of this study include designing hollow gold nanoparticles as a carrier of MTX, and using high power LED (3 W) for photodynamic therapy with HAuNP.

2. Materials and methods

2.1. Chemicals

Mitoxantrone hydrochloride (MW = 517.4), trisodium citrate dehydrate (> 99%), chloroauric acid ($HAuCl_4{\cdot}4H2O$), cobalt chloride hexahydrate (99.99%), methoxy-polyethylene-glycol (mPEG-SH, MW = 2000), MTT (3-[4,5-dimethylthiazol-2-yl]-2,5-diphenyltetrazolium bromide), trypan blue, RPMI 1640, penicillin, trypsin–EDTA, streptomycin, and sodium borohydride (99%) were purchased from Sigma-Aldrich (St. Louis, MO, USA).

2.2. Cell culture

MCF7 (human breast adenocarcinoma cell line) and DFW (Melanoma cell line) cells were purchased from Pasteur Institute of Iran. These cell lines were cultured in RPMI 1640 containing fetal bovine serum (10%), streptomycin (100 µg/ml), and penicillin (100 units/ml). A carbon dioxide incubator with atmospheric conditions of 5% CO_2 and temperature of 37 °C was used for cell growth.

2.3. Instrumentations

The main equipment used in this study were incubator CO_2, Elisa reader (AWARENESS, USA), milwaukee pH-thermo Meter (MT609, Italy), radiometer (CON-TROL-CURE IL1400, USA), UV–Vis spectrophotometer (UNICO UV-2100, USA), Dynamic-Light-Scattering (DLS) particle size analyzer (Nano-ZS, Malvern, UK), light emitting diode (633 ± 13 nm; 3 W), PHILIPS CM120 and Transmission electron microscope (TEM).

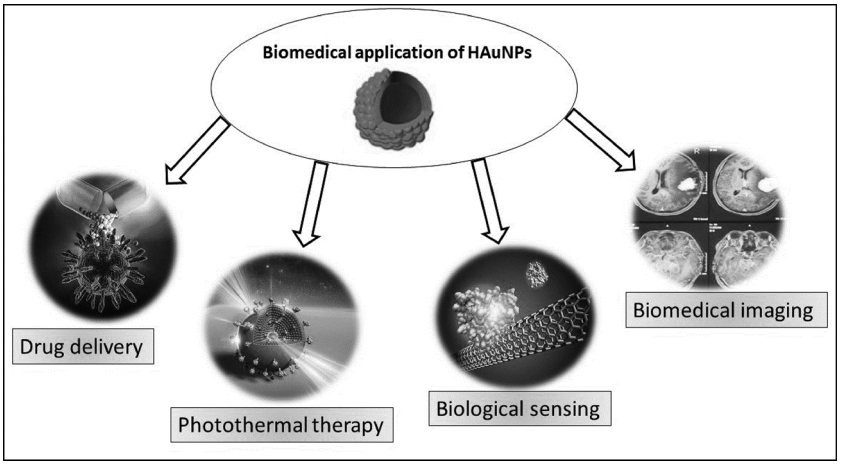

Fig. 1. Important Biomedical Application of hollow gold nanoparticle.

2.4. Synthesis of HAuNP and PEGylation

First of all, it should be noted that the water used in all steps of the synthesis process must have three important features: ultra-purity, sterility, and de-oxygenation. The use of nitrogen (or argon) gas flux during the synthesis process is required to preclude the entry of oxygen.

The first step in the process of synthesizing HAuNP is the synthesis of oxygen-sensitive cobalt nanoparticles (OSCNs) as the sacrificial core. For this purpose, 120 µl of 0.1 M sodium citrate solution and 30 µl of 1 M sodium tetrahydroborate solution were added to 30 ml of deoxygenated ultra-pure water simultaneously. After a few seconds, with the addition of 30 µl of a 0.4 M cobalt chloride solution, a dark brown solution appeared due to the synthesis of OSCNs. The process time depends on the initial water temperature, with higher temperatures accelerating the synthesis process of OSCNs.

In the next step, OSCNs were immediately transferred to a vortexing solution with 10 ml of deoxygenated ultra-pure water containing 25 µl of 0.1 M chloroauric acid. In this reaction, the gold shell was formed on the surface of cobalt core. Finally, the solution was exposed to air or oxygen flux for oxidization and removal of the cobalt core. The fact that the color of solution changed from dark brown to green indicated the oxidation of OSCNs, which eventually led to formation of HAuNP (NP). To pegylate the hollow gold nanoparticles (P-NP), a 200 µl aqueous solution of methoxy-PEG was added to 19.8 ml of the HAuNPs solution, and the resulting solution was incubated on the magnet stirrer at room temperature for 4 h. The solutions were then centrifuged at 1000*g* for 15 min. The supernatant was gradually discarded to remove excess methoxy-PEG, and then added up to 15 ml of PBS solution (Fig. 2).

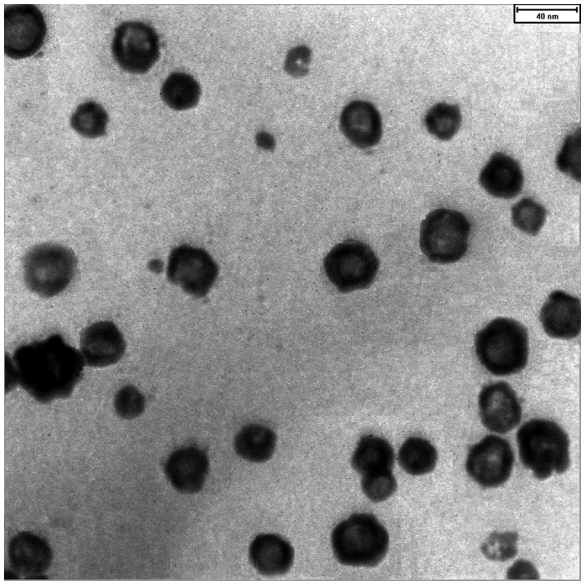

Fig. 3. TEM image of synthesized hollow gold nanoparticles.
Hollow gold nanoparticles have a surface plasmon resonnace band in the visible up to the infrared, depending on the shell thickness to the core ratio.

2.5. Characterization of MTX and nanostructures

The absorption spectra of MTX, NP, and P-NP were recorded by an UV–Vis spectrophotometer. The particle size distribution, conductivity, zeta potential, and PDI (polydispersity index) of the nanostructures were determined using a DLS. TEM imaging was used to examine the morphology of nanostructures.

2.6. Conjugation and release process of MTX

The entrapment of the drug in hollow gold nanoparticles is conducted in two steps: 1) drug conjugation into the cavity space of

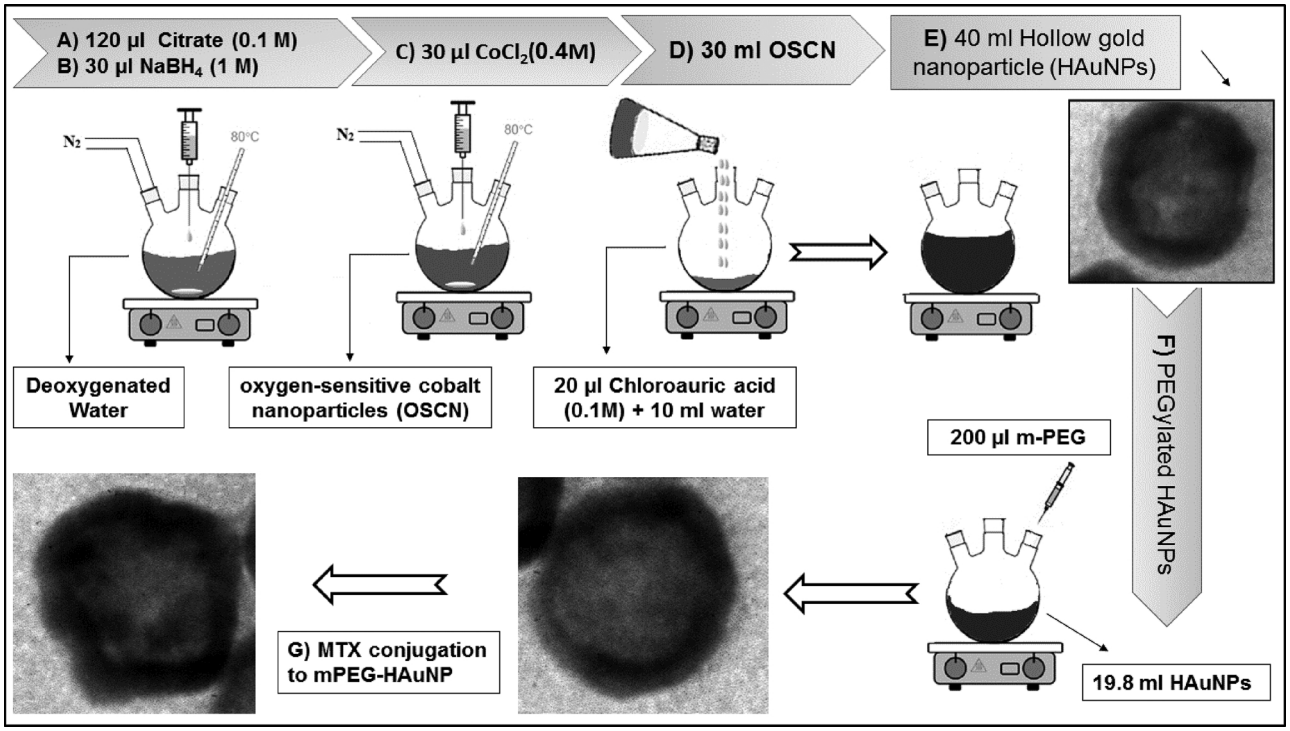

Fig. 2. Synthesis scheme of hollow gold nanoparticle and final product.
Notes: (A,B) 120 µl of 0.1 M sodium citrate solution and 30 µl of 1 M sodium tetrahydroborate solution were added to 30 ml of deoxygenated ultra-pure water simultaneously. **(C)** addition of 30 µl of a 0.4 M cobalt chloride solution (Synthesis of oxygen-sensitive cobalt nanoparticle). **(D)** OSCNs were immediately transferred to a vortexing solution of 10 ml of deoxygenated ultra-pure water containing 25 µl of 0.1 M chloroauric acid. **(E)** Formation of hollow gold nanoparticles. **(F)** 200 µl aqueous solution of methoxy-PEG was added to 19.8 ml of the HAuNPs solution. **(G)** MTX conjugation to mPEG-HAuNP.

Table 1
Physical characteristics of Nanostructures (pH = 7).

Nanostructure	Size (nm)	PDI	Conductivity (mS/cm)	Zatta potential (mV)	Dis. medium viscosity (mPa s)
NP	43 ± 4	0.300	0.173	−21.6	0.892
P-NP	58 ± 7	0.291	0.069	−0.2	0.892
MTX-P-NP	63 ± 4	0.348	0.273	−12.4	0.892

nanoparticles and 2) drug sticking (conjugation) to the internal or external surface of nanoparticles. In this study, the drug trapping process represents a type of conjugation, and the drug release process reveals the loosening of drug bonds from the surface of nanoparticles and their spreading to the surrounding area of nanoparticles.

Spectrophotometric and spectrofluorimetric analyzes were used to evaluate the conjugation and release process of MTX from the nanostructures. To study the conjugation process, absorption and fluorescence spectra of MTX@mPEG-HAuNP (MTX-P-NP) were recorded over the drug conjugation process before, during and 24 h after conjugation. Along with the analysis of drug release, MTX-P-NP (3.5×10^{11} particles/mL at 630 nm) was placed in a quartz cuvette, irradiated with an LED system (630 nm; 3 W) with radiant exposure of 0.4, 1.3 and 3.9 J/cm^2; and subjected to spectrofluorometric analysis immediately after irradiation by LED with a Shimadzu spectrofluorometric (Nakagyo-ku, Japan) at an excitation wavelength of 607 nm and emission spectrum of 665–705 nm.

2.7. In vitro experiments

DFW cells (melanoma cancer cell line) and MCF-7 (human breast cancer cell line) were seeded into 24-well plates with cell densities of 7.5×10^4 (For DFW) and 9.0×10^4 (For MCF-7) cells per well and cultured at CO_2 incubator for 24 h. Then, the culture medium was replaced with a fresh medium containing nanostructures (NP, P-NP, and MTX-P-NP) of varying concentrations. After 90 min incubation, the plates were washed twice with PBS to remove the excess unbond nanostructures, and then a fresh culture medium (with 3% FBS) was added to each plate well. Afterward, the cells were exposed to different radiant exposure (0.4, 1.3, and 3.9 J/cm^2; 630 nm). After cell irradiation by LED, a fresh culture medium (with 17% FBS) was added to wells (FBS was adjusted to (3 + 17)/2 = 10%) and incubation lasted for 24 h. Finally, MTT assay was performed for all treatment groups 24 h after treatment. The following formula was used to calculate the radiant exposure: (power density (irradiance) of LED = 7.25 mW/cm^2)

radiant exposure (J/cm^2) = irradiance (W/cm^2) × time of irradiation (s)

Thus, after microscopic examination of the morphology, cell growth or cell death in the control and treatment groups, and ensuring the absence of microbial contamination, the cell culture medium was discharged under the laminar hood. After the medium without FBS, which contained 50 µl of MTT solution (5 mg/ml), was added to the wells under dark conditions, the plates were covered with aluminum foil and placed in the incubator. After 4 h, 200 µl DMSO (Dimethyl sulfoxide) was added to dissolve formazan crystals. Then, to ensure the uniformity of solutions, each plate was placed on a stirrer for 5 min and their optical densities were read at 570 nm and compared to that of 630 nm.

2.8. Evaluation indices

Three indices were used to compare the results as follows:

The concentration required to obtain a cell death of 50% under dark condition was determined by IC_{50}. The light radiant exposure required to obtain 50% cell death in the irradiant group was considered with ED_{50}. Treatment Efficacy (TE) was described as the ratio of radiation-induced cell death (CD) in the presence of MTX-P-NP to radiation-induced cell death in the presence of MTX. It was defined to compare the therapeutic efficacy of the treatment.

$$TE(MTX-mPEG-HAuNP) = \frac{CD(MTX-mPEG-HAuNP)}{CD(MTX)}$$

2.9. Statistical analysis

SPSS 20 software was used for data analysis. The survival curves of the treatment groups were plotted by Excel software. The normality of data was assessed by the non-parametric Kolmogorov-Smirnov test.

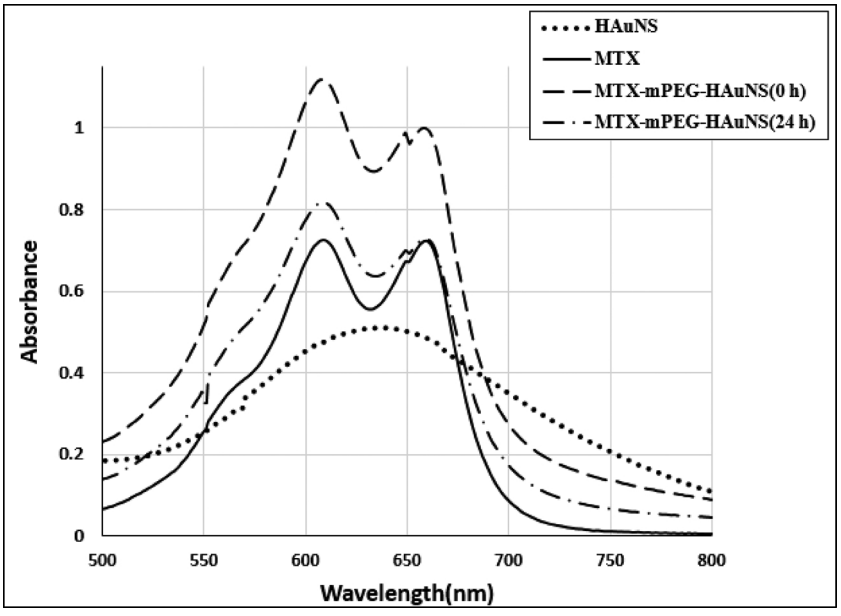

Fig. 4. Spectrophotometric analysis during the conjugation time of the drug.
Absorption spectrum during the conjugation process of MTX to mPEG-HAuNP. after completion of the conjugate process, the OD decreases, which is due to the bonding of the drug to the nanoparticle surface.

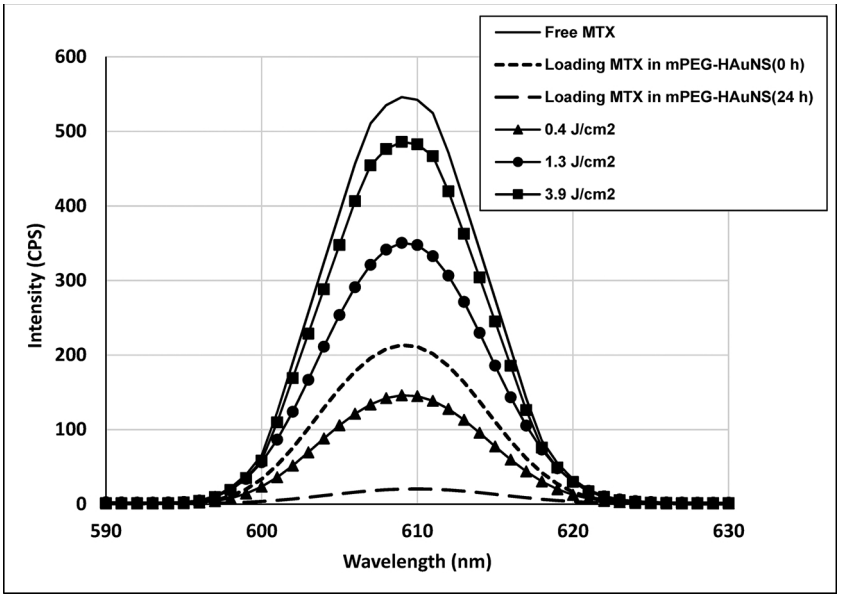

Fig. 5. Fluorescence signal variations during the MTX conjugation process and Radiation of different light expoxures. An increase in the fluorescence signal level after radiation can be due to the release of the drug.

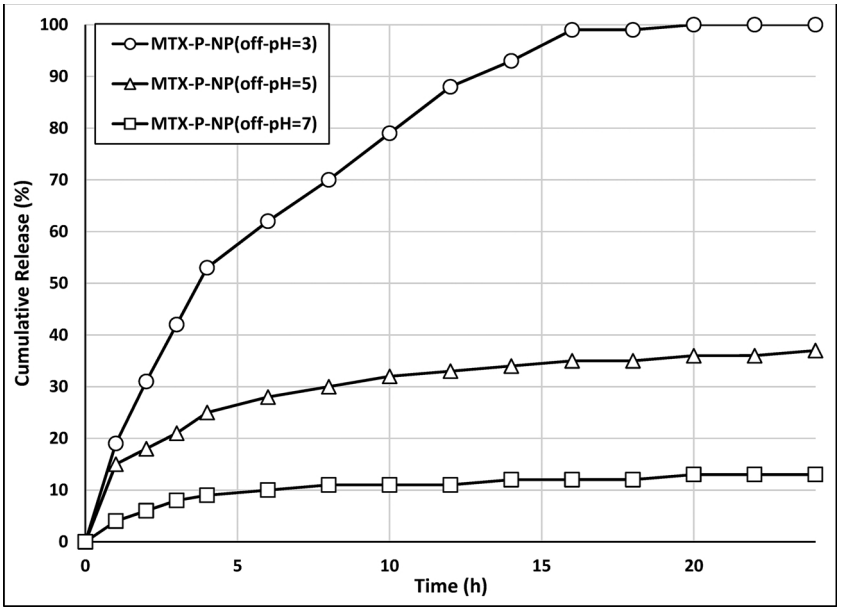

Fig. 6. MTX release profiles in the absence of LED Exposure at different pH. Reducing the pH leads to rapid MTX release from MTX-N-NP without exposure.

Given the normality of data distribution, Tukey test and one-way ANOVA were employed to compare mean differences.

3. Results

3.1. Synthesis of MTX-P-NP

The results of transmission electron microscopy (TEM) indicated that the synthesized nanostructure was hollow with an average diameter of 40 nm (Fig. 3). Physical characteristics of different nanostructures including size, Zetta potential, and poly dispersity index (PDI) are shown in Table 1. To investigate the effect of PEGylation process and conjugation MTX on HAuNP, physical factors were examined in relation to each other. These factors included dispersion medium viscosity, conductivity and zeta potential. The dispersion medium viscosity factor was identical for NP, P-NP and MTX-P-NP. The reason is that after the PEGylation/conjugation process and centrifugation of the resulting solution, the mPEG/drug that had not bonded with nanoparticles were removed from the solution. If the centrifuging was not performed after the PEGylation/conjugation, the viscosity of environment would vary due to the presence of free mPEG and (or) MTX. The surface modification by methoxy-polyethylene-glycol (mPEG), which increased the average size of HAuNP from 43 ± 4 to 58 ± 7 nm, led to a reduction of conductivity from 0.173 mS/ cm to 0.069 mS/cm, and thus zeta potential was positive and close to zero. Considering the above factors, we concluded that the PEGylation process changed the physical properties of the initial HAuNP. These results confirmed the completion of surface modification process. The PEGylation of HAuNP improved their physicochemical stability in the aqueous media. As a result, their stability was increased from 30 days to 4 months, but no aggregation was observed at room temperature. The absorption spectra suggested that the surface plasmon resonance for both NP and P-NP was

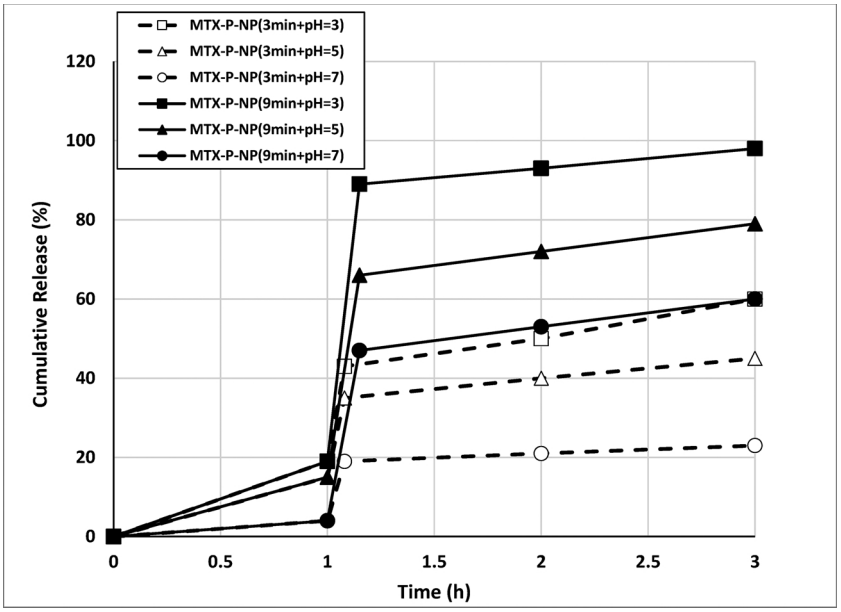

Fig. 7. MTX release profiles in the presence of LED Exposure at different pH.
Irradiation with LED caused rapid MTX release from MTX-N-NP during LED exposure (3,9 min), and the release was turned off when LED was switched off.

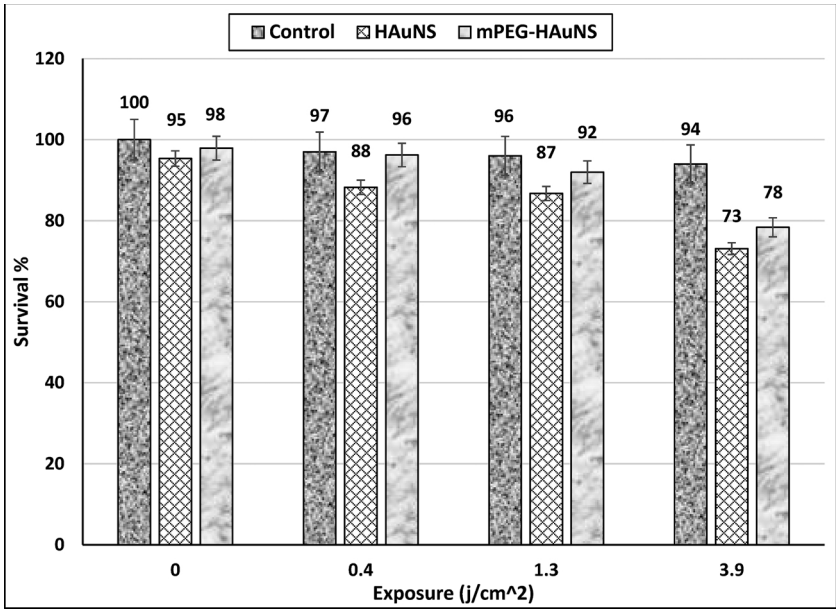

Fig. 8. Cell survival percentage 24 h after different irradiation conditions in the presence of the HAuNP and mPEG-HAuNP (NP, P-NP) in MCF-7 cells. Data has shown mean ± SD (n = 6).

tuned at 630 nm.

Fig. 4 shows the absorption spectra of different nanostructures during the MTX conjugation process. 24 h after mixing, the OD of MTX-P-NP in the UV–vis region dropped compared to the OD immediately after mixing of MTX-P-NP (0 h). The optical density was lost over time due to greater and stronger binding of the drug to nanoparticles. The conjugation process increased the size of nanoparticles up to 63 nm, changed conductivity to 0.273 mS/cm, and decreased Zeta's potential from about zero to −12.4 mV.

3.2. MTX release from MTX-P-NP

Free MTX exhibited strong fluorescence emission. At the outset of MTX conjugation process, the fluorescence signal of MTX-P-NP was lower than the free MTX. After 24 h, the fluorescence signal of MTX-P-NP was almost completely quenched. This usually occurs when fluorophores are conjugated to or enclosed within the nanostructure. This finding reveals the strong binding of the MTX to nanostructures (Fig. 5).

To assess colloidal stability, we examined the release rate of MTX from P-NP at a medium with different pH. Endosomes and intracellular lysosomes are acidic (pH of approximately 5.0), and this acidity can facilitate active drug release from delivery vehicles based on nanostructures. LED irradiation increased the amount of MTX released from MTX-P-NP, which was incubated in PBS at different pH levels. After an initial release of 10% over the first 4 h, no further release of MTX from either MTX-P-NP was observed in the phosphate-buffered saline (PBS, pH 7.0) after 1 day. The results indicated that MTX was absorbed to P-NP in a stable manner. However, when pH dropped, the amount of drug release was significantly increased, so that at pH = 3 and about 15 h, all of the MTX was released from MTX-P-NP (Fig. 6). MTX release from

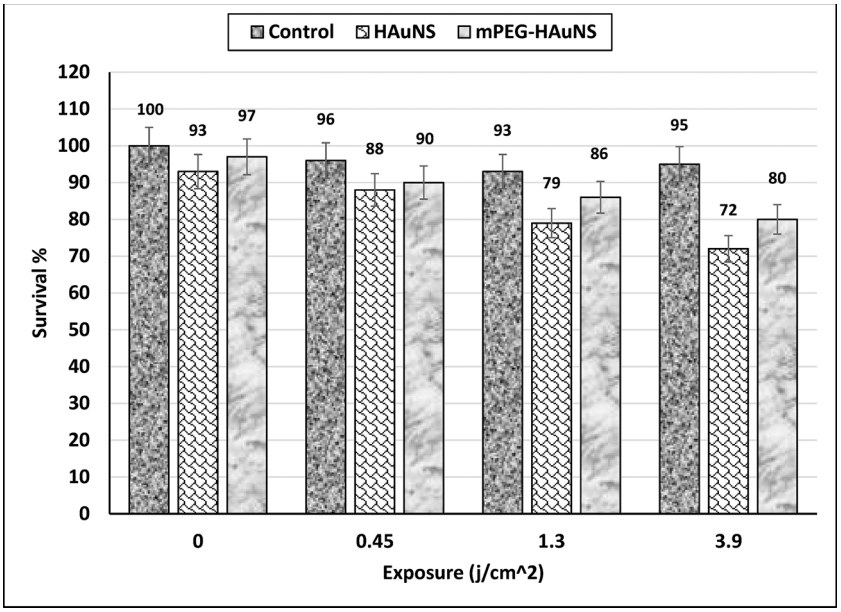

Fig. 9. Cell survival percentage 24 h after different irradiation conditions in the presence of the HAuNP and mPEG-HAuNP (NP, P-NP) in DFW cells. Data has shown mean ± SD (n = 6).

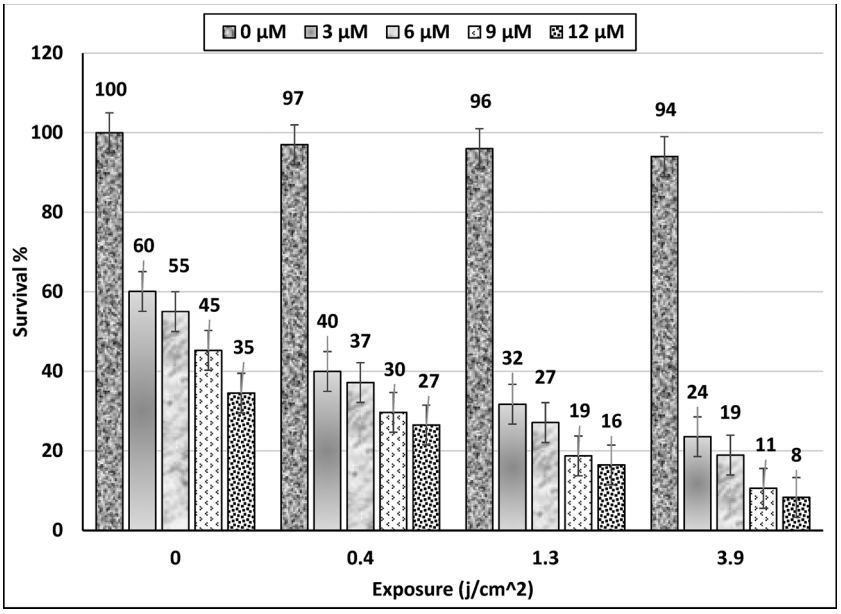

Fig. 10. Cell survival percentage 24 h after different irradiation conditions in the presence of the MTX in MCF-7.

MTX-P-NP could be controlled using LED. After LED irradiation at a different pH, the cumulative release (defined as the ratio of released MTX to total conjugated MTX expressed as a percentage) increased. The release rate of MTX was significantly reduced when the LED radiant exposure was switched off. The data suggested that MTX release from MTX-P-NP could be triggered by LED radiant exposure (Fig. 7).

3.3. Effects of LED irradiation with NP and P-NP

In Figs. 8 and 9, the percentages of cell survival at different radiant exposure times in the absence of therapeutic agents (control groups) as well as dark toxicity at different concentrations of agents are shown. The comparison of cell viability in the absence of therapeutic agents (Except radiant exposure group of 1.3 J/cm^2) did not show any significant difference between DFW and MCF-7 cell lines at lower and higher radiant exposure ($P > 0.05$). According to Figs. 8 and 9, it can be concluded that under dark conditions, these nanostructures are non-toxic in concentrations used in this study (3.5×10^{11} particles/mL). In both cell lines, the highest cell death was observed at 3.9 J/cm^2 of radiant exposure for NP and P-NP groups. The functionalized nanoparticles (PEGylated nanoparticles) have lower toxicity compared to non-PEGylated nanoparticles. This can be due to the biocompatibility of PEG.

3.4. Effects of LED irradiation in the presence of MTX

By examining the relevant group of cytotoxicity under different conditions in the presence of MTX in MCF-7 (Fig. 10), we observed that the effect of PDT-induced toxicity was intensified by increasing concentrations or radiant exposures. This feature is due to specific optical properties of the MTX, which presents it as a photosensitizer.

In DFW as compared to MCF-7, MTX is less effective under dark

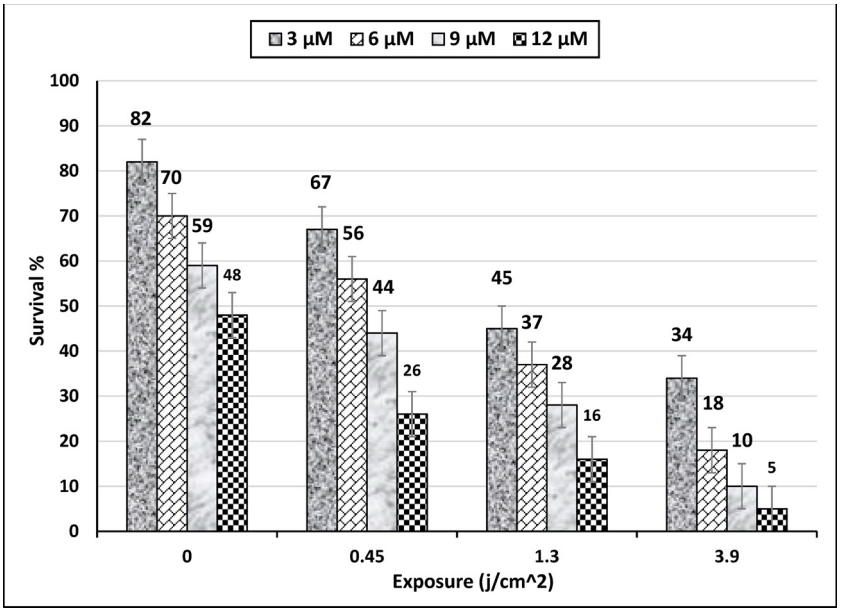

Fig. 11. Cell survival percentage 24 h after different irradiation conditions in the presence of the MTX in DFW.

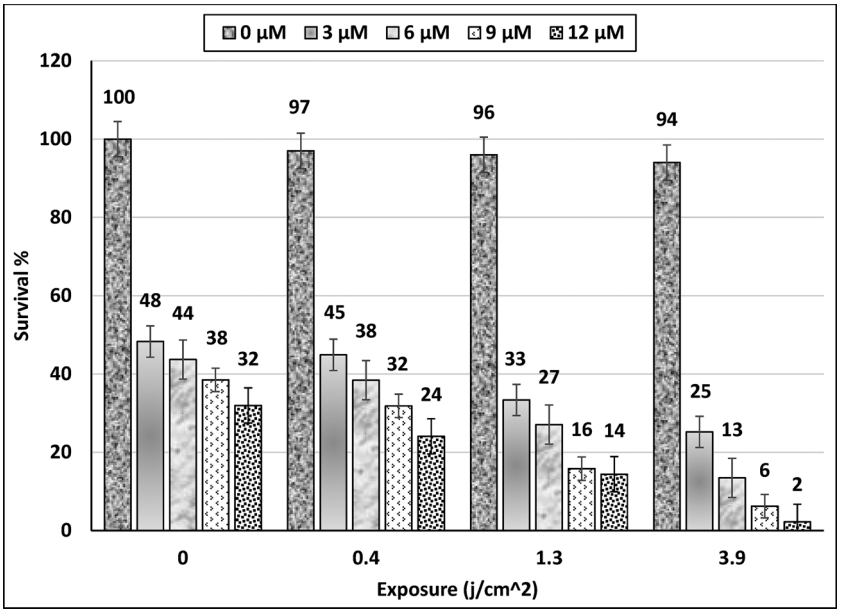

Fig. 12. Cell survival percentage 24 h after different irradiation conditions in the presence of the MTX-mPEG-HAuNP (MTX-P-NP) in MCF-7.

conditions and cellular survival is relatively higher ($P < 0.05$). However, by increasing concentrations, cell death also increased (Fig. 11). The comparison of cell death under dark conditions and after 9 min of radiant exposure (≈3.9 J/cm^2) between the two cell lines revealed that free MTX had a greater phototoxic effect on DFW compared to that of MCF7 ($P < 0.05$).

3.5. Effects of LED irradiation in the presence of MTX-P-NP

A comparison of Figs. 10–13 suggests that MTX-P-NP cytotoxicity is greater than that of free MTX at all concentrations ($P < 0.05$). However, the difference is more significant at lower concentrations (less than 6 µM) ($P \approx 0.000$). In the DFW cell line, the cell death rate at concentrations of 3–6 µM under dark conditions before reaching a radiant exposure of 1.3 J/cm^2 was lower than that of MCF-7 cell line for the same condition ($P < 0.05$). However, by increasing the irradiation time, the percentage of cellular survival of DFW dropped lower than MCF7 cell survival. For concentrations higher than 9 µM, however, the cell death in DFW was higher than that of MCF7 for similar conditions under both dark and radiant conditions ($P < 0.05$) (Figs. 12 & 13).

4. Discussion

As far as we are concerned, there is a paucity of studies on the use of hollow gold nanoparticles conjugated with MTX. Several studies on the same subject were examined and finally evaluated based on defined indices.

Tan Boon et al. synthesized polyhedron nanostructures consisting of carbon (Nanodiamonds; NDs) as a carrier of MTX. NDs-MTX significantly increased the MTX cellular uptake in MDA-MB-231 cells (which are resistant to MTX). The release of MTX from NDs was strongly influenced by pH changes and concentration of soluble proteins in the environment. The main goal of those studies was to inhibit the expression of efflux receptors in breast cancer cells (ABCG2), which

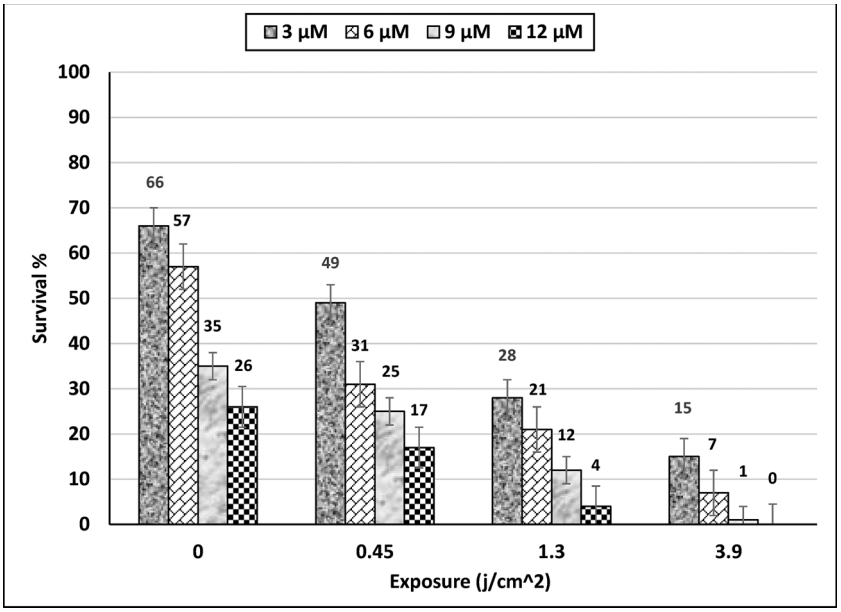

Fig. 13. Cell survival percentage 24 h after different irradiation conditions in the presence of the MTX-mPEG-HAuNP (MTX-P-NP) in DFW.

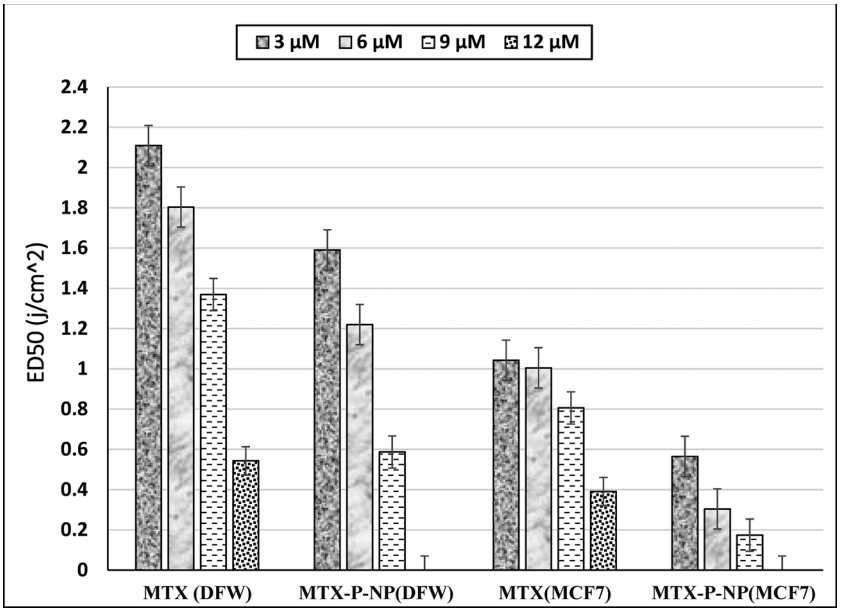

Fig. 14. ED_{50} Indexes of the agents in DFW and MCF-7.
ED_{50}: The light exposure required to obtain 50% cell death in the irradiant group.

pumped drug out of the cell. Using NDs-MTX, efflux pumps were inhibited and therapeutic efficacy was increased [15].

Barrar et al. designed PEG-FA-MTX-MNPs nanostructures based on magnetic nanoparticles (MNPs), which formed a covalent bond with MTX, folic acid (FA), and polyethylene glycol (PEG). This nanostructure was used to eradicate cancer cells with folate receptor. Their findings revealed that after the uptake of PEG-FA-MTX-MNPs nanostructures by cancer cells with folate receptors, which destroys target cancer cells by increasing the expression of BCL-2 and Caspase9 and reducing the expression of Akt, the above nanostructure was proposed for simultaneous imaging and treatment of various cancers that were over-expressed by folate receptors [16].

Hornung et al. investigated the effect of super-paramagnetism of iron oxide conjugated to MTX on the HT-29 cell line. They found that free MTX did not have any significant effect on tumor growth inhibition, but the SPION-MTX nanostructure inhibited tumor growth [17].

Jian Yu et al. investigated the photothermal effect of doxorubicin-conjugated hollow gold nanosphere (HAUNP) by an infrared laser. They reported that the PEG increased the efficiency of drug conjugation in HAuNP. In fact, a dual-purpose therapeutic approach was suggested as the chemo-photothermal therapy [18].

To evaluate the performance of MTX-P-NP as drug carriers, various indices such as IC_{50}, ED_{50}, and TE were studied.

The IC50 index was used to determine the essential concentration of a treatment agent to reach a cell death of 50% under dark conditions. The lower IC50 of specific agent was due to its higher toxicity compared to other agents under similar conditions. ED_{50} also indicated the degree of light exposure that caused 50% cell death at a specified concentration. For some concentrations, the cell survival under dark conditions was less than 50% and thus it was impossible to calculate the ED50. To overcome this problem, ED_{50} was considered as zero for MTX-P-NP with the maximum concentration (12µM) that induced the highest cell

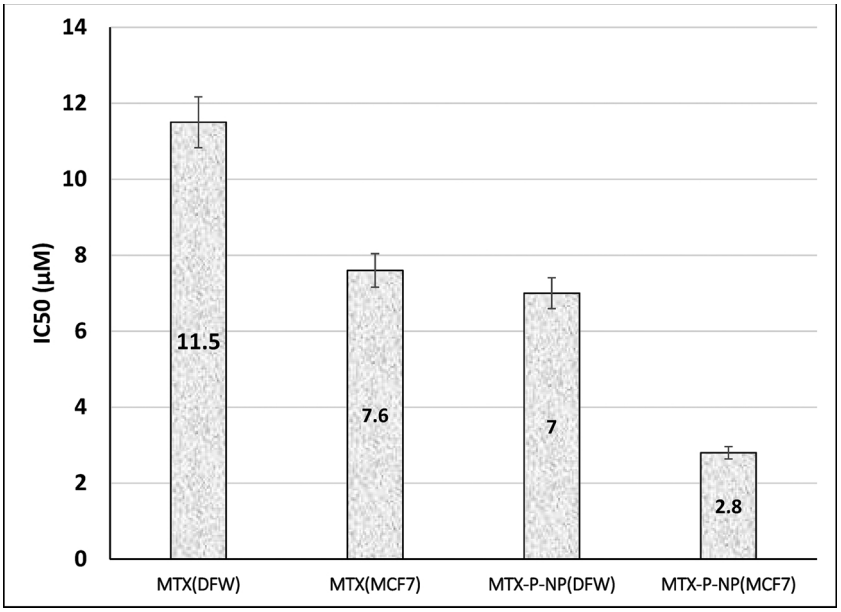

Fig. 15. IC_{50} Indexes of the agents in DFW and MCF-7.
IC_{50}: The concentration required to obtain a cell death of 50% under dark condition.

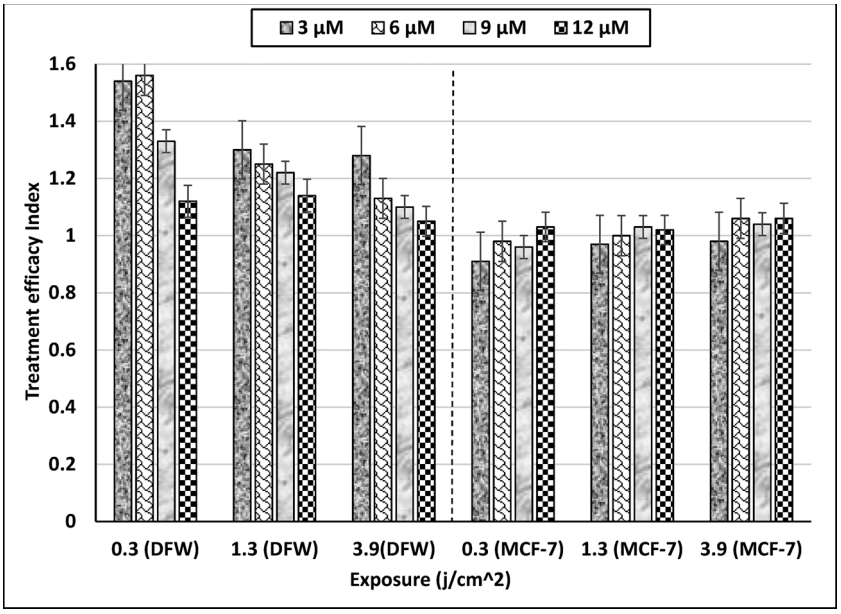

Fig. 16. Treatment efficacy index (TE) of the agents in MCF-7 and DFW cells.
Treatment Efficacy (TE) was described as the ratio of radiation-induced cell death (CD) in the presence of MTX-P-NP to radiation-induced cell death in the presence of MTX.
$(\mathrm{TE(MTX-mPEG-HAuNP)} = \frac{CD(\mathrm{MTX-mPEG-HAuNP})}{CD(MTX)})$.

death, and other factors were normalized. In both cell lines (Figs. 14 & 15), the combination of IC50 and ED50 results suggested that the MTX-P-NP with higher cellular uptake (higher UC) resulted in higher effective cellular toxicity (lower IC_{50}) and optical sensitivity (lower ED_{50}).

To find the amount of drug conjugation in the nanostructure that improved the therapeutic efficacy of MTX, TE index was used. In the MCF-7 cell line (Fig. 16), no significant change was observed in MTX-P-NP of different radiant exposures and concentrations, and in all cases, TE was about 1. The maximum TE ($\approx$1.05) for MTX-P-NP was observed at a radiant exposure of 3.9 J/cm^2 and concentration of 12 μM. Unlike MCF-7 cell line, the conditions were different for the DFW cell line (Fig. 16). In all concentrations and exposures of light, TE index of MTX-P-NP was greater than 1. The maximum TE ($\approx$1.56) for MTX-P-NP was observed at a radiant exposure of 1.3 J/cm^2 and concentration of 6 μM.

5. Conclusion

Among nanostructures of various morphologies and types, hollow gold nanoparticles have unique capabilities for multimodal treatments (including chemotherapy, PDT and photothermal therapy) due to features such as spherical shape, small size, tunable near-infrared absorption peak area, convenient surface modification with a variety of targeted biological molecules and desirable biocompatibility. This is the first study to use hollow gold nanoparticles as carriers for MTX. The mitoxantrone was chosen for the interesting optical properties of MTX to improve the photodynamic process. Also, based on the tunable

absorption peak of HAuNP, it is possible to improve the optical properties of MTX with the aim of inducing photodynamic effects through conjugation of this drug into HAuNP. The main findings of this study are:

1) The PEGylation of the HAuNP improved cellular uptake and increased conjugation capacity of the MTX.
2) The effect of photodynamic-chemotherapy of MTX-mPEG-HAuNP on the DFW cell line was significantly greater than that of MCF-7. This can be attributed to the specific resistance mechanisms of the breast cell lines.
3) The release of TMX from the mPEG-HAuNS is dependent on the time of radiant and as well as the pH of the environment.

Conflict of interest

There is no conflict of interest to report.

Acknowledgement

The authors would like to thank the research deputy of Mashhad University of Medical Sciences for funding this research. The results described in this paper are a part of an MSc Medical physics thesis.

References

[1] R.R. Allison, H.C. Mota, C.H. Sibata, Clinical PD/PDT in North America: an historical review, Photodiagn. Photodyn. Ther. 1 (4) (2004) 263–277.
[2] A.P. Castano, T.N. Demidova, M.R. Hamblin, Mechanisms in photodynamic therapy: part one—photosensitizers, photochemistry and cellular localization, Photodiagn. Photodyn. Ther. 1 (4) (2004) 279–293.
[3] C.A. Robertson, D.H. Evans, H. Abrahamse, Photodynamic therapy (PDT): a short review on cellular mechanisms and cancer research applications for PDT, J. Photochem. Photobiol. B Biol. 96 (1) (2009) 1–8.
[4] A. Erkiert-Polguj, A. Halbina, I. Polak-Pacholczyk, H. Rotsztejn, Light-emitting diodes in photodynamic therapy in non-melanoma skin cancers–own observations and literature review, J. Cosmet. Laser Ther. 18 (2) (2016) 105–110.
[5] J. Hempstead, D.P. Jones, A. Ziouche, G.M. Cramer, I. Rizvi, S. Arnason, et al., Low-cost photodynamic therapy devices for global health settings: characterization of battery-powered LED performance and smartphone imaging in 3D tumor models, Sci. Rep. 5 (2015) 10093.
[6] R.V.J. Chari, Targeted Cancer therapy: conferring specificity to cytotoxic drugs, Acc. Chem. Res. 41 (1) (2008) 98–107.
[7] S.N. Khan, S.K. Lal, P. Kumar, A.U. Khan, Effect of mitoxantrone on proliferation dynamics and cell-cycle progression, Biosci. Rep. 30 (6) (2010) 375–381.
[8] A.-R. Montazerabadi, A. Sazgarnia, M.H. Bahreyni-Toosi, A. Ahmadi, A. Shakeri-Zadeh, A. Aledavood, Mitoxantrone as a prospective photosensitizer for photodynamic therapy of breast cancer, Photodiagn. Photodyn. Ther. 9 (1) (2012) 46–51.
[9] R. Fanciullino, J. Ciccolini, G. Milano, Challenges, expectations and limits for nanoparticles-based therapeutics in cancer: a focus on nano-albumin-bound drugs, Crit. Rev. Oncol. Hematol. 88 (3) (2013) 504–513.
[10] Y. Zhang, F. Huang, C. Ren, L. Yang, J. Liu, Z. Cheng, et al., Targeted chemo-photodynamic combination platform based on the DOX prodrug nanoparticles for enhanced cancer therapy, ACS Appl. Mater. Interfaces 9 (15) (2017) 13016–13028.
[11] Q.-Q. Ren, L.-Y. Bai, X.-S. Zhang, Z.-Y. Ma, B. Liu, Y.-D. Zhao, et al., Preparation, modification, and application of hollow gold nanospheres, J. Nanomater. (2015) (2015) 7.
[12] M.P. Melancon, W. Lu, Z. Yang, R. Zhang, Z. Cheng, A.M. Elliot, et al., In vitro and in vivo targeting of hollow gold nanoshells directed at epidermal growth factor receptors for photothermal ablation therapy, Mol. Cancer Ther. 7 (6) (2008) 1730–1739.
[13] N.J. Butcher, G.M. Mortimer, R.F. Minchin, Unravelling the stealth effect, Nat. Nanotechnol. 11 (2016) 310.
[14] Y. Cheng, A.C. Samia, J. Li, M.E. Kenney, A. Resnick, C. Burda, Delivery and efficacy of a cancer drug as a function of the bond to the gold nanoparticle surface, Langmuir 26 (4) (2010) 2248–2255.
[15] T.-B. Toh, D.-K. Lee, W. Hou, L.N. Abdullah, J. Nguyen, D. Ho, et al., Nanodiamond–mitoxantrone complexes enhance drug retention in chemoresistant breast cancer cells, Mol. Pharm. 11 (8) (2014) 2683–2691.
[16] J. Barar, V. Kafil, M.H. Majd, A. Barzegari, S. Khani, M. Johari-Ahar, et al., Erratum to: multifunctional mitoxantrone-conjugated magnetic nanosystem for targeted therapy of folate receptor-overexpressing malignant cells, J. Nanobiotechnol. 13 (1) (2015) 59.
[17] A. Hornung, M. Poettler, R.P. Friedrich, B. Weigel, S. Duerr, J. Zaloga, et al., Toxicity of mitoxantrone-loaded superparamagnetic iron oxide nanoparticles in a HT-29 tumour spheroid model, Anticancer Res. 36 (6) (2016) 3093–3101.
[18] J. You, G. Zhang, C. Li, Exceptionally high payload of doxorubicin in hollow gold nanospheres for near-infrared light-triggered drug release, ACS Nano 4 (2) (2010) 1033–1041.